

2019

# Measurement of the Beam Spin Asymmetry of $\rightarrow ep \rightarrow e'p'\eta$ in the Deep-Inelastic Regime with CLAS

B. Zhao

A. Kim


K. Joo

I. Bedlinskiy

W. Kim

*See next page for additional authors*

Follow this and additional works at: [https://digitalcommons.odu.edu/physics\\_fac\\_pubs](https://digitalcommons.odu.edu/physics_fac_pubs)

 Part of the [Atomic, Molecular and Optical Physics Commons](#), and the [Plasma and Beam Physics Commons](#)

## Repository Citation

Zhao, B.; Kim, A.; Joo, K.; Bedlinskiy, I.; Kim, W.; Kubarovsky, V.; Ungaro, M.; Gavalian, G.; Klein, A.; Kuhn, S. E.; and CLAS Collaboration, "Measurement of the Beam Spin Asymmetry of  $\rightarrow ep \rightarrow e'p'\eta$  in the Deep-Inelastic Regime with CLAS" (2019). *Physics Faculty Publications*. 356.

[https://digitalcommons.odu.edu/physics\\_fac\\_pubs/356](https://digitalcommons.odu.edu/physics_fac_pubs/356)

## Original Publication Citation

Zhao, B., Kim, A., Joo, K., Bedlinskiy, I., Kim, W., Kubarovsky, V., . . . Zhao, Z. W. (2019). Measurement of the beam spin asymmetry of  $\rightarrow ep \rightarrow e'p'\eta$  in the deep-inelastic regime with CLAS. *Physics Letters B*, 789, 426-431. doi:10.1016/j.physletb.2018.12.065

---

**Authors**

B. Zhao, A. Kim, K. Joo, I. Bedlinskiy, W. Kim, V. Kubarovsky, M. Ungaro, G. Gavalian, A. Klein, S. E. Kuhn,  
and CLAS Collaboration



## Measurement of the beam spin asymmetry of $\vec{e}p \rightarrow e'p'\eta$ in the deep-inelastic regime with CLAS



B. Zhao<sup>a,b</sup>, A. Kim<sup>a,\*</sup>, K. Joo<sup>a</sup>, I. Bedlinskiy<sup>c</sup>, W. Kim<sup>d</sup>, V. Kubarovskiy<sup>e,f</sup>, M. Ungaro<sup>e</sup>, S. Adhikari<sup>g</sup>, Z. Akbar<sup>h</sup>, G. Angelini<sup>i</sup>, H. Avakian<sup>e</sup>, J. Ball<sup>j</sup>, N.A. Baltzell<sup>e,k</sup>, L. Barion<sup>l</sup>, M. Bashkanov<sup>m</sup>, M. Battaglieri<sup>n</sup>, V. Batourine<sup>e,d</sup>, A.S. Biselli<sup>o,p</sup>, S. Boiarinov<sup>e</sup>, W.J. Briscoe<sup>i</sup>, W.K. Brooks<sup>q,e</sup>, V.D. Burkert<sup>e</sup>, D.S. Carman<sup>e</sup>, A. Celentano<sup>n</sup>, P. Chatagnon<sup>r</sup>, T. Chetry<sup>s</sup>, G. Ciullo<sup>l,t</sup>, L. Clark<sup>u</sup>, B.A. Clary<sup>a</sup>, P.L. Cole<sup>v</sup>, M. Contalbrigo<sup>l</sup>, V. Crede<sup>h</sup>, A. D'Angelo<sup>w,x</sup>, N. Dashyan<sup>y</sup>, R. De Vita<sup>n</sup>, E. De Sanctis<sup>z</sup>, M. Defurne<sup>j</sup>, A. Deur<sup>e</sup>, S. Diehl<sup>a</sup>, C. Djalali<sup>k</sup>, R. Dupre<sup>r</sup>, H. Egiyan<sup>e,aa</sup>, M. Ehrhart<sup>r</sup>, A. El Alaoui<sup>q</sup>, L. El Fassi<sup>ab</sup>, P. Eugenio<sup>h</sup>, A. Filippi<sup>ac</sup>, T.A. Forest<sup>v</sup>, G. Gavalian<sup>e,ad</sup>, Y. Ghandilyan<sup>y</sup>, G.P. Gilfoyle<sup>ae</sup>, F.X. Girod<sup>e,j</sup>, E. Golovatch<sup>af</sup>, R.W. Gothe<sup>k</sup>, K.A. Griffioen<sup>b</sup>, M. Guidal<sup>r</sup>, L. Guo<sup>g,e</sup>, K. Hafidi<sup>ag</sup>, H. Hakobyan<sup>q,y</sup>, N. Harrison<sup>e</sup>, M. Hattawy<sup>ag</sup>, D. Heddle<sup>ah,e</sup>, K. Hicks<sup>s</sup>, M. Holtrop<sup>aa</sup>, Y. Ilieva<sup>k,i</sup>, D.G. Ireland<sup>u</sup>, B.S. Ishkhanov<sup>af</sup>, E.L. Isupov<sup>af</sup>, D. Jenkins<sup>ai</sup>, H.S. Jo<sup>d,r</sup>, S. Johnston<sup>ag</sup>, M.L. Kabir<sup>ab</sup>, D. Keller<sup>aj</sup>, G. Khachatryan<sup>y</sup>, M. Khachatryan<sup>ad</sup>, M. Khandaker<sup>ak,1</sup>, A. Klein<sup>ad</sup>, F.J. Klein<sup>al</sup>, S.E. Kuhn<sup>ad</sup>, S.V. Kuleshov<sup>q,c</sup>, L. Lanza<sup>w</sup>, P. Lenisa<sup>l</sup>, K. Livingston<sup>u</sup>, I.J.D. MacGregor<sup>u</sup>, D. Marchand<sup>r</sup>, N. Markov<sup>a</sup>, B. McKinnon<sup>u</sup>, C.A. Meyer<sup>p</sup>, Z.E. Meziani<sup>am</sup>, M. Mirazita<sup>z</sup>, V. Mokeev<sup>e,af</sup>, R.A. Montgomery<sup>u</sup>, C. Munoz Camacho<sup>r</sup>, P. Nadel-Turonski<sup>e,i</sup>, S. Niccolai<sup>r</sup>, G. Niculescu<sup>an</sup>, M. Osipenko<sup>n</sup>, A.I. Ostrovidov<sup>h</sup>, M. Paolone<sup>am</sup>, R. Parenduyan<sup>aa</sup>, K. Park<sup>e,d</sup>, O. Pogorelko<sup>c</sup>, J.W. Price<sup>ao</sup>, Y. Prok<sup>ad,e</sup>, D. Protopopescu<sup>u</sup>, M. Ripani<sup>n</sup>, A. Rizzo<sup>w,x</sup>, G. Rosner<sup>u</sup>, P. Rossi<sup>e,z</sup>, F. Sabatié<sup>j</sup>, C. Salgado<sup>ak</sup>, R.A. Schumacher<sup>p</sup>, Y.G. Sharabian<sup>e</sup>, Iu. Skorodumina<sup>k,af</sup>, G.D. Smith<sup>m</sup>, D. Sokhan<sup>u</sup>, N. Sparveris<sup>am</sup>, S. Stepanyan<sup>e</sup>, I.I. Strakovskiy<sup>i</sup>, S. Strauch<sup>k,i</sup>, M. Taiuti<sup>ap,2</sup>, J.A. Tan<sup>d</sup>, H. Voskanyan<sup>y</sup>, E. Voutier<sup>r</sup>, R. Wang<sup>r</sup>, X. Wei<sup>e</sup>, M.H. Wood<sup>aq,k</sup>, N. Zachariou<sup>m</sup>, J. Zhang<sup>aj,ad</sup>, Z.W. Zhao<sup>ar</sup>

<sup>a</sup> University of Connecticut, Storrs, CT 06269, United States of America

<sup>b</sup> College of William and Mary, Williamsburg, VA 23187-8795, United States of America

<sup>c</sup> Institute of Theoretical and Experimental Physics, Moscow, 117259, Russia

<sup>d</sup> Kyungpook National University, Daegu 41566, Republic of Korea

<sup>e</sup> Thomas Jefferson National Accelerator Facility, Newport News, VA 23606, United States of America

<sup>f</sup> Rensselaer Polytechnic Institute, Troy, NY 12180-3590, United States of America

<sup>g</sup> Florida International University, Miami, FL 33199, United States of America

<sup>h</sup> Florida State University, Tallahassee, FL 32306, United States of America

<sup>i</sup> The George Washington University, Washington, DC 20052, United States of America

<sup>j</sup> IRFU, CEA, Université Paris-Saclay, F-91191 Gif-sur-Yvette, France

<sup>k</sup> University of South Carolina, Columbia, SC 29208, United States of America

<sup>l</sup> INFN, Sezione di Ferrara, 44100 Ferrara, Italy

<sup>m</sup> Edinburgh University, Edinburgh EH9 3JZ, United Kingdom

<sup>n</sup> INFN, Sezione di Genova, 16146 Genova, Italy

<sup>o</sup> Fairfield University, Fairfield CT 06824, United States of America

<sup>p</sup> Carnegie Mellon University, Pittsburgh, PA 15213, United States of America

<sup>q</sup> Universidad Técnica Federico Santa María, Casilla 110-V Valparaíso, Chile

\* Corresponding author.

E-mail address: [kenjo@jlab.org](mailto:kenjo@jlab.org) (A. Kim).

<sup>1</sup> Current address: Pocatello, Idaho 83209.

<sup>2</sup> Current address: 16146 Genova, Italy.

<sup>r</sup> Institut de Physique Nucléaire, CNRS/IN2P3 and Université Paris Sud, Orsay, France

<sup>s</sup> Ohio University, Athens, OH 45701, United States of America

<sup>t</sup> Università di Ferrara, 44121 Ferrara, Italy

<sup>u</sup> University of Glasgow, Glasgow G12 8QQ, United Kingdom

<sup>v</sup> Idaho State University, Pocatello, ID 83209, United States of America

<sup>w</sup> INFN, Sezione di Roma Tor Vergata, 00133 Rome, Italy

<sup>x</sup> Università di Roma Tor Vergata, 00133 Rome, Italy

<sup>y</sup> Yerevan Physics Institute, 375036 Yerevan, Armenia

<sup>z</sup> INFN, Laboratori Nazionali di Frascati, 00044 Frascati, Italy

<sup>aa</sup> University of New Hampshire, Durham, NH 03824-3568, United States of America

<sup>ab</sup> Mississippi State University, Mississippi State, MS 39762-5167, United States of America

<sup>ac</sup> INFN, Sezione di Torino, 10125 Torino, Italy

<sup>ad</sup> Old Dominion University, Norfolk, VA 23529, United States of America

<sup>ae</sup> University of Richmond, Richmond, VA 23173, United States of America

<sup>af</sup> Skobeltsyn Institute of Nuclear Physics, Lomonosov Moscow State University, 119234 Moscow, Russia

<sup>ag</sup> Argonne National Laboratory, Argonne, IL 60439, United States of America

<sup>ah</sup> Christopher Newport University, Newport News, VA 23606, United States of America

<sup>ai</sup> Virginia Tech, Blacksburg, VA 24061-0435, United States of America

<sup>aj</sup> University of Virginia, Charlottesville, VA 22901, United States of America

<sup>ak</sup> Norfolk State University, Norfolk, VA 23504, United States of America

<sup>al</sup> Catholic University of America, Washington, DC 20064, United States of America

<sup>am</sup> Temple University, Philadelphia, PA 19122, United States of America

<sup>an</sup> James Madison University, Harrisonburg, VA 22807, United States of America

<sup>ao</sup> California State University, Dominguez Hills, Carson, CA 90747, United States of America

<sup>ap</sup> Università di Genova, 16146 Genova, Italy

<sup>aq</sup> Canisius College, Buffalo, NY, United States of America

<sup>ar</sup> Duke University, Durham, NC 27708-0305, United States of America

## ARTICLE INFO

### Article history:

Received 9 August 2018

Received in revised form 6 December 2018

Accepted 28 December 2018

Available online 3 January 2019

Editor: V. Metag

### Keywords:

Nucleon structure

CLAS collaboration

Deeply Virtual Meson Production

Chiral-odd generalized parton distributions

## ABSTRACT

The beam spin asymmetry of the exclusive pseudoscalar channel  $\bar{e}p \rightarrow e'p'\eta$  was measured for the first time in the deep-inelastic regime ( $W > 2 \text{ GeV}/c^2$  and  $Q^2 > 1 \text{ GeV}^2/c^2$ ) using a longitudinally polarized 5.78 GeV electron beam at Jefferson Lab with the CEBAF Large Acceptance Spectrometer. The data were accumulated in 144 four-dimensional bins of  $Q^2$ ,  $x_B$ ,  $-t$  and  $\phi$  over a wide kinematic range, where  $\phi$  is the azimuthal angle between the lepton and hadron scattering planes. The measured azimuthal dependence with large amplitudes of the  $\sin\phi$  moments is a clear indication of a substantial contribution to the polarized cross-section from transversely polarized virtual photons. In the framework of generalized parton distributions (GPDs) this contribution is expressed via longitudinal-transverse interference between chiral-even and chiral-odd GPDs. The experimental results are compared to the existing theoretical models demonstrating the sensitivity to the product of chiral-odd and chiral-even GPDs and provide new constraints to the existing GPD parameterizations.

© 2019 The Authors. Published by Elsevier B.V. This is an open access article under the CC BY license (<http://creativecommons.org/licenses/by/4.0/>). Funded by SCOAP<sup>3</sup>.

Deeply virtual exclusive processes with high photon virtuality  $Q^2$  have emerged as a powerful probe to study nucleon structure at the parton level. These processes include deeply virtual Compton scattering (DVCS) and deeply virtual meson production (DVMP), which can be described as convolutions of hard parton processes and soft generalized parton distributions (GPDs) within QCD factorization theorems (see Fig. 1). These GPDs represent the non-perturbative nucleon structure, unifying the concepts of hadronic form factors and parton distributions [1,2]. They also provide access to hitherto unexplored observables such as the spatial distributions of partons of a given longitudinal momentum fraction or the orbital angular momentum of quarks and gluons inside the nucleon. While DVCS, which has been extensively studied both theoretically [1–4] and experimentally [5–13], is the main channel for constraining the GPDs at leading twist, DVMP allows one to uniquely access certain GPDs that involve higher twist mechanisms.

In general, there are four chiral-even GPDs ( $H$ ,  $\tilde{H}$ ,  $E$ ,  $\tilde{E}$ ) involved in the parton helicity-conserving processes and four chiral-odd GPDs, which correspond to the parton helicity-flip processes ( $H_T$ ,  $\tilde{H}_T$ ,  $E_T$ ,  $\tilde{E}_T$ ). At leading twist in the GPD framework, the neutral pseudoscalar DVMP, e.g. exclusive  $\pi$  and  $\eta$  production, amplitudes couple only to longitudinally polarized photons. Therefore these channels are sensitive only to the chiral even GPDs  $\tilde{H}$  and  $\tilde{E}$

in the nucleon [14,15]. These two GPDs are difficult to isolate in DVCS alone [16]. The early theoretical efforts to explain pseudoscalar DVMP focused on these  $\tilde{H}$  and  $\tilde{E}$  GPDs at leading twist, ignoring the contribution from transverse virtual photons. However, these calculations failed to describe the experimental data from Jefferson Lab [17–20] and HERMES [21,22] for exclusive pion electroproduction, underestimating the measured cross sections by more than an order of magnitude. This stimulated the development of theoretical models that calculate chiral-odd quark helicity-flip subprocesses, in order to evaluate the role of transverse photon polarization components in the description of the neutral pseudoscalar DVMP channels [23]. Recent theoretical work showed that transverse virtual photon contributions can be calculated within a handbag approach as the convolution of the leading-twist chiral-odd GPDs with a twist-3 meson distribution amplitude [24–26]. This fact makes pseudoscalar meson production the key process to study, constrain and extract chiral-odd GPDs.

The number of available experimental observables is not enough to isolate contributions from the different GPDs in a model independent way. While chiral-even GPDs are better known from available experimental data, such as DVCS, which gives the most direct access to GPDs, deep inelastic scattering via parton distribution functions, and nucleon form factors measurements, their chiral-odd counterparts are far less constrained. The variety of

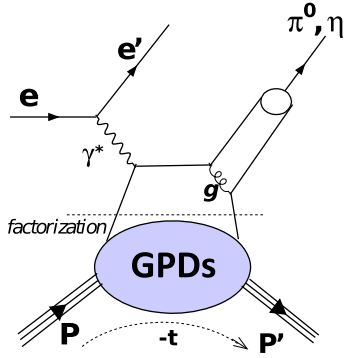


Fig. 1. The leading-order handbag diagram of neutral pseudoscalar meson production. The symbol  $g$  represents the gluon that is exchanged between quark lines.

DVMP channels produces a large number of experimental observables that are sensitive to different combinations of the chiral-odd GPDs, and their different flavor combinations allow one to perform the decomposition of the underlying quark GPDs. Under the GPD formalism, the relevance of the  $\pi^0$  and the  $\eta$  beam spin asymmetry (BSA) dataset comparison is particularly important. The treatment of the electroproduction of  $\pi^0$  and  $\eta$  mesons within the handbag approach is similar, but the GPDs appear in the following flavor combinations:

$$\begin{aligned} F^{\pi^0} &= (e_u F^u - e_d F^d) / \sqrt{2} \\ F^\eta &= (e_u F^u + e_d F^d) / \sqrt{6} \end{aligned} \quad (1)$$

where  $F$  stands for any previously introduced GPD, and  $u$  and  $d$  indexes are the up and down quark GPDs, and  $e_u$  and  $e_d$  their respective charges. Therefore, the combined analysis of these two reactions enables one to perform a quark flavor separation. To achieve this separation it is necessary to accumulate as many relevant channels in the same kinematic range, and with similar binning, for the global analysis to constrain quark GPDs. This paper describes a step in this direction.

The GPDs can be accessed through of a variety of channels including differential cross sections, beam and target polarization asymmetries in exclusive meson production [27–29]. Polarized beam asymmetries measurements are reported here. The beam spin asymmetry is defined as follows:

$$A_{LU} = \frac{d\sigma^+ - d\sigma^-}{d\sigma^+ + d\sigma^-} = \frac{\alpha \sin \phi}{1 + \beta \cos \phi + \gamma \cos 2\phi}, \quad (2)$$

where the index  $LU$  denotes a longitudinally polarized beam and unpolarized target.  $d\sigma^+$  and  $d\sigma^-$  are the differential cross sections for the beam helicity, aligned and anti-aligned to the beam direction, respectively.  $\phi$  is the azimuthal angle between the lepton and hadron scattering planes, on which the differential cross sections depend. The parameter  $\alpha$  is proportional to the polarized structure function  $\sigma_{LT'}$ , which is due to the interference between the amplitudes for longitudinal ( $\gamma_L^*$ ) and transverse ( $\gamma_T^*$ ) virtual photon polarizations:

$$\alpha = \frac{\sqrt{2\epsilon(1-\epsilon)}\sigma_{LT'}}{\sigma_T + \epsilon\sigma_L}, \quad (3)$$

where  $\sigma_L$  and  $\sigma_T$  are the structure functions that correspond to longitudinal and transverse virtual photons, and variable  $\epsilon$  represents the ratio of their fluxes.

The single spin polarized structure functions are constructed using the products of GPD convolutions ( $\langle F \rangle \langle F_T \rangle$ ), where  $\langle F \rangle$

and  $\langle F_T \rangle$  represent the chiral-even and chiral-odd GPD convolutions (see Fig. 1), respectively. Therefore, any sizable BSA measurements would indicate that the BSA amplitudes receive substantial contributions from both types of GPDs.

Indeed, the measurements by the CLAS Collaboration of large single and double spin asymmetry values for deep exclusive  $\pi^0$  electroproduction over a wide kinematic region [18,30,31] and of the unpolarized structure functions for exclusive  $\pi^0$  and  $\eta$  electroproduction [19,32,33], indicate a dominance of transverse photon amplitudes in the pseudoscalar channels, and a strong sensitivity to the chiral-odd GPDs. In this letter, we present the first time measurements of the beam spin asymmetry for exclusive  $\eta$  electroproduction.

The measurements were carried out in the spring of 2005 using the CEBAF Large Acceptance Spectrometer (CLAS) [34–38] located in Hall B at Jefferson Lab. The data were collected with a 5.776 GeV longitudinally polarized electron beam and a 2.5 cm long liquid-hydrogen target. The target was placed inside a superconducting solenoid magnet of 4.5 Tesla to shield the detectors from Møller electrons, focusing them towards the beam line, while allowing detection of photons from  $4.5^\circ$  and maintaining the minimum permitted angle for electrons and protons at  $21^\circ$ .

The large acceptance of the CLAS spectrometer allowed simultaneous detection of all four final-state particles of the  $\bar{e}p \rightarrow e'p'\eta$  reaction, with the  $\eta$  meson reconstructed by measuring the  $2\gamma$  decay channel. The scattered electron was identified by reconstructing the track in the drift chambers (DC) and matching it in time with signals in the electromagnetic calorimeter (EC) and Cherenkov counters. The cuts on the EC energy deposition effectively suppressed the background from negative pions, and the tracks near the detector edges were excluded using geometrical cuts. The proton was identified as a positively charged particle track in the DC with the correct time-of-flight information from the scintillation counters. The  $\eta$  meson decay photons were detected using both the EC and the inner calorimeter (IC) installed downstream of the target. The former covered angles greater than  $17^\circ$  while the latter enabled the detection of forward photons in the angular range from  $5^\circ$  to  $17^\circ$ . The photons were identified as neutral particles with cuts on the minimum energy of 0.15 GeV and the speed  $\beta > 0.95$ . Additionally, a geometric cut was applied to exclude the detector edges, where the energy of the photons was not fully reconstructed.

After the identification of the four final state particles, the following steps were followed to reconstruct exclusive events from the  $\bar{e}p \rightarrow e'p'\eta$  reaction. Since the four-momenta of all final-state particles were measured, tight *exclusivity* cuts were applied to ensure energy and momentum conservation. These cuts rejected the events from other reactions such as  $\pi^0$ ,  $\rho$ , and  $\omega$  production, or where any additional undetected particles were present. For  $\eta$  decay, the following photon-detection topologies were recognized: both photons detected in the IC (IC-IC), both photons in the EC (EC-EC), the higher energy photon in the IC and lower energy photon in the EC (IC-EC), the higher energy photon in the EC and lower energy photon in the IC (EC-IC). The *exclusivity* cuts were determined independently for each topology. As expected, the IC-IC topology had the best resolution due to the superior IC performance, while the EC-EC topology had the lowest. Then, four cuts were used for the selection of events from exclusive  $\eta$  meson production:

- (i)  $|M_X^2(e'p') - M_\eta^2| < 3\sigma$ , where  $M_X^2(e'p')$  is the missing mass squared of the  $ep$  system in  $ep \rightarrow e'p'X$ ;
- (ii)  $|M_X^2(e'\gamma\gamma) - M_\eta^2| < 3\sigma$ , where  $M_X^2(e'\gamma\gamma)$  is the missing mass squared of the  $e'\gamma\gamma$  system in  $ep \rightarrow e'\gamma\gamma X$ ;

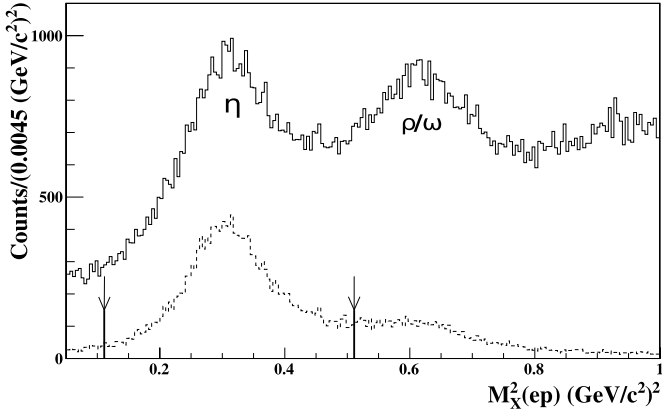


**Fig. 2.** Distributions of missing mass squared of the  $(e'p')$  system for the reaction  $ep \rightarrow e'p'\eta$  before applying the exclusivity cuts (solid line) and after applying the  $3\sigma$  cuts on  $M_X^2(e'\gamma\gamma)$  and the cone angle  $\theta_{\eta X}$  (dashed). The two arrows indicate the  $3\sigma$  cut on this distribution.

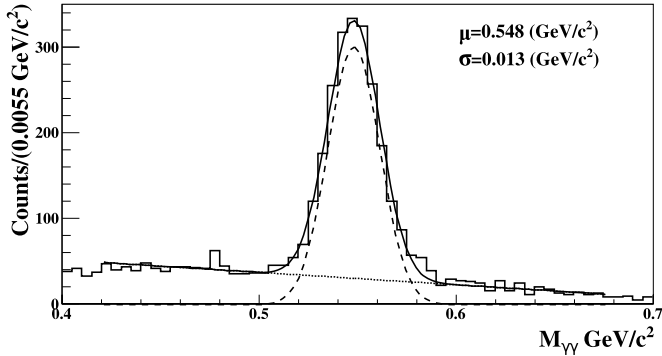


**Fig. 3.** The distribution of  $\eta$  invariant mass ( $M_{\gamma\gamma}$ ) in a representative  $\phi$  bin ( $90^\circ \leq \phi < 120^\circ$ ) of the IC-IC configuration, fit by a Gaussian function (dashed line) plus a linear background (dotted line). The solid line is the sum of both contribution.

- (iii)  $|M_{\gamma\gamma} - M_\eta| < 3\sigma$ , where  $M_{\gamma\gamma}$  is the invariant mass of the two photons;
- (iv)  $\theta_{\eta X} < 1.3^\circ, 2.5^\circ, 1.6^\circ, 2^\circ$  for the IC-IC, EC-EC, IC-EC and EC-IC topologies, respectively, where  $\theta_{\eta X}$  is the cone angle between the measured and the kinematically reconstructed  $\eta$  meson in the  $(ep \rightarrow e'p'X)$  system.

Here  $\sigma$  is the observed experimental resolution obtained as the standard deviation from the mean value of the distributions of each quantity.

Fig. 2 shows the effect of the exclusivity cuts on the missing mass squared of the  $ep$  system, and demonstrates the reduction of contamination from different meson production channels. The invariant mass  $M_{\gamma\gamma}$  spectrum is shown in Fig. 3 for IC-IC topology in a representative  $\phi$  bin. Even after the application of the other exclusivity cuts, the  $M_{\gamma\gamma}$  distribution contains a small amount of background under the  $\eta$  mass peak. The shape of the invariant mass distribution suggests that the background under the  $\eta$  peak can be parametrized using a linear function and, therefore, can be subtracted using the sideband method. The data in the sidebands ( $-6\sigma, -3\sigma$ ) and  $(3\sigma, 6\sigma)$  of the  $M_{\gamma\gamma}$  distributions were used to estimate the number of background events under the  $\eta$  peak for each  $\{Q^2, x_B, -t, \phi\}$  kinematic bin and helicity state and were subtracted.

To ensure that the selected events were from the deep-inelastic regime, cuts on the invariant mass of the  $\gamma^*p$  pair  $W$  and on the photon virtuality  $Q^2$  were applied:  $W > 2 \text{ GeV}/c^2$ ,  $Q^2 >$

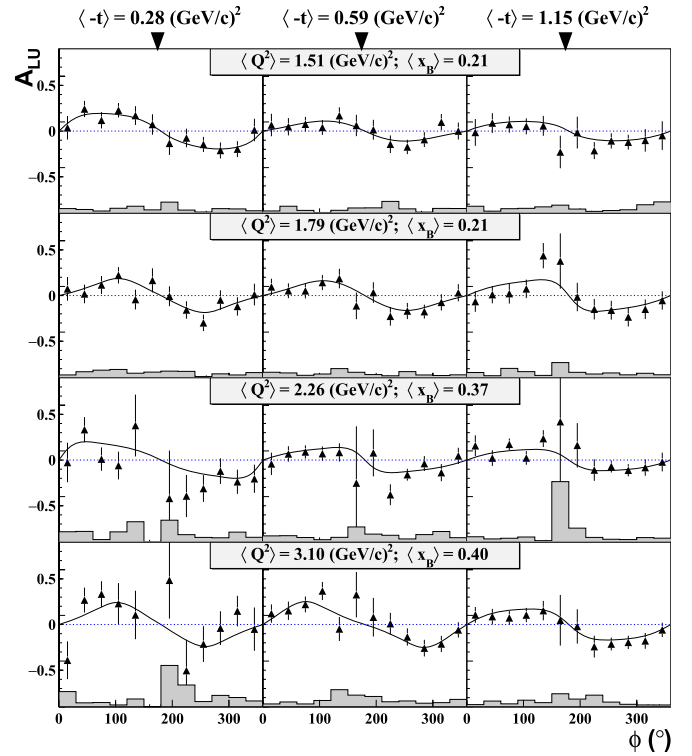


**Fig. 4.** Beam spin asymmetries (BSA) for deep exclusive  $\eta$  production plotted as a function of  $\phi$  for three dimensional bins  $\{Q^2, x_B\}$  (rows) and  $-t$  (columns). The BSAs are fit with the function in Eq. (2). The shaded bands represent the overall systematic uncertainties.

$1 \text{ (GeV}/c^2)$ . The selected events were then divided into 144 four-dimensional kinematical bins, with 4 bins in  $\{Q^2, x_B\}$ , 3 bins in  $-t$ , and 12 bins in  $\phi$ , for each of the two possible beam helicities, where  $x_B = \frac{Q^2}{2p \cdot q}$  is the Bjorken variable,  $t = (p - p')^2$  is the four momentum transfer to the nucleon, and  $p$  and  $p'$  are the initial and final four-momenta of the nucleon. From these data samples, the beam spin asymmetries were calculated for each bin as:

$$A_{LU} = \frac{1}{P_b} \frac{n^+ - n^-}{n^+ + n^-}, \quad (4)$$

where  $n^{+(-)}$  are the number of events for each beam helicity, normalized by the corresponding beam luminosity, and  $P_b$  is the average beam polarization value.

Using the sideband subtraction method the background removal was performed independently for each beam helicity and thus takes into account the background asymmetry. The bin centering corrections were also applied although their effect was negligible.

The beam polarization  $P_b$  was measured several times during the experiment using the Hall B Møller polarimeter [34]. The absolute average value was calculated as  $79.4 \pm 3.5\%$  using the beam polarization measurements weighted by all the events.

The beam spin asymmetry for exclusive  $\eta$  production was measured over a kinematic range with  $Q^2 = 1-4.5 \text{ (GeV}/c^2)$ ,  $x_B = 0.1-0.58$ ,  $-t = 0.1-1.8 \text{ (GeV}/c^2)$ . The computed asymmetries are shown in Fig. 4. The azimuthal dependence of the measured  $A_{LU}$  was fit using the function in Eq. (2). However, due to the low statistics, the coefficients  $\beta$  and  $\gamma$  were not well constrained. In order to achieve good quality fits, limits were applied to the parameters  $\beta$  and  $\gamma$ . The limits were determined empirically by first observing the fits performed without constraints. It was found that, although the parameters  $\beta$  and  $\gamma$  in the denominator were affected by the low statistics, the  $\sin\phi$  amplitude  $\alpha$  was stable.

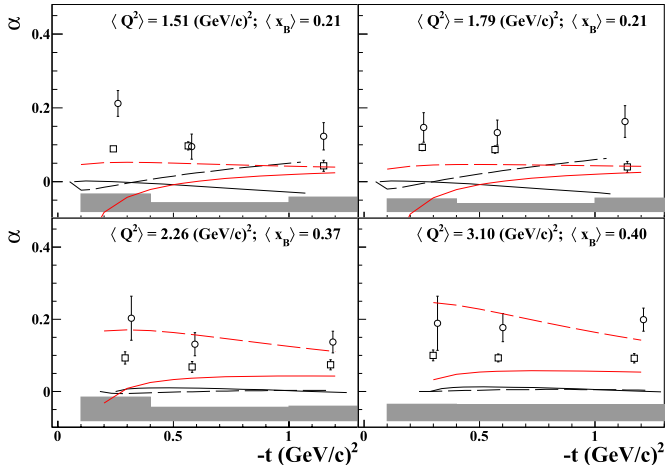


**Fig. 5.** The fit parameter  $\alpha$  for the beam spin asymmetry of exclusive  $\eta$  (open circles) and  $\pi^0$  (open squares) electroproduction as a function of  $-t$  for 4 bins in  $\{Q^2, x_B\}$ . The shaded bands represent the systematic uncertainties for the  $\eta$  beam spin asymmetry measurements. The curves show the calculations for  $\eta$  (solid) and for  $\pi^0$  (dashed) from two GPD models: GK [24] (black) and GGL [25] (red).

The systematic uncertainties associated with the fit were evaluated using three fitting procedures: the  $\sin\phi$  modulation was extracted with free  $\beta$  and  $\gamma$  parameters, with limits on  $\beta$  and  $\gamma$ , and with 1-parameter fits with  $\beta = \gamma = 0$ . In all cases the parameter  $\alpha$  showed very small variations in comparison with the statistical uncertainties. This effect was included in the overall systematic uncertainty.

The extraction of the beam spin asymmetry for exclusive  $ep \rightarrow e'p'\eta$  reaction includes several sources of systematic uncertainties. The main sources are the event selection procedures, particularly the exclusivity cuts on  $M_X^2(ep)$ ,  $M_X^2(e\gamma\gamma)$  and  $\theta_{\eta X}$ . The BSA was measured with these cuts modified from  $1.5\sigma$  to  $4.5\sigma$ , and the corresponding BSA variation was used to assign systematic uncertainties, which were evaluated on a bin-by-bin basis and estimated to be 0.075 on average. The background asymmetry and its deviation from the linear shape lead to a systematic uncertainty of 0.033. The relative systematic uncertainty of the beam polarization leads to a global normalization uncertainty and contributes around 0.035. The individual systematic uncertainties were combined, and the overall uncertainty is conservatively estimated at 0.087. The systematic uncertainties are shown as the gray shaded bands for each kinematic bin in Figs. 4 and 5.

In Fig. 5, the extracted  $\alpha$  for  $\eta$  production are plotted as a function of  $-t$  in each  $\{Q^2, x_B\}$  bin. They are compared with previously reported measurements of deep exclusive  $\pi^0$  electroproduction [18], explicitly rebinned according to this analysis. The main feature of the beam spin asymmetry is a rather flat behavior in both  $-t$  and  $Q^2$ , where the latter can be ascribed to approximate Bjorken scaling. The interpretation of the  $-t$  dependence is particularly interesting since its flat slope in  $-t$  provides an opportunity to constrain the dependence of the underlying GPDs at large  $-t$ . Combined with the unpolarized cross section measurements we can access the product of  $H_T$  and  $\tilde{E}$ , thus allowing us to separate the real and imaginary parts of the chiral-odd GPD convolutions. Also, the large amplitudes of the  $\sin\phi$  moments suggest that the interference term between longitudinally and transversely polarized virtual photons is significantly underestimated in current theoretical models.

Fig. 5 includes the theoretical predictions from two GPD-based models by Goloskokov–Kroll (GK) [24] and Goldstein–Gonzalez–Liuti (GGL) [26]. Both models calculate the contributions from the transverse ( $\gamma_T^*$ ) virtual photon amplitudes using chiral-odd

GPDs with their  $-t$  dependence incorporated from Regge phenomenology. The main difference between these models is their GPD parametrization methods. The GGL model produces the chiral-odd GPD parametrization via linear relations to chiral-even GPDs under parity and charge conjugation symmetries in their Reggeized diquark model. This approach allows them to overcome the fact that very few constraints on chiral-odd GPDs exist, while chiral-even GPDs can be relatively well-constrained using deep inelastic scattering, nucleon form-factor and DVCS measurements. In the GK model, chiral-odd GPDs are constructed from the double distributions and constrained using the latest results from lattice QCD and transversity parton distribution function with the emphasis on  $H_T$  and  $\tilde{E}_T$ , while the contribution from other chiral-odd GPDs are considered negligible.

Neither model accounts for the large beam spin asymmetry values. The GGL model predicts a large BSA for the high  $Q^2$  and  $x_B$  bins for  $\pi^0$ , while in the GK model the asymmetries are very small. The difference in magnitudes between the two models arises from the various GPD contributions to the longitudinally polarized beam structure function  $\sigma_{LT'}$ . According to the GPD formalism,  $\sigma_{LT'}$  contains the products of chiral-even and chiral-odd GPDs. In the GK model the dominant term is  $\text{Im}\{(H_T)^*(\tilde{E})\}$ , and other contributions are neglected, while the GGL model calculates amplitudes sensitive to  $\text{Im}\{(E_T)^*(\tilde{H})\}$  producing relatively large BSA values, especially in the high  $Q^2$  and  $x_B$  region. For  $\eta$  production,  $\langle E_T^u \rangle$  and  $\langle E_T^d \rangle$  are expected to cancel each other due to the different quark flavor composition, as shown in Eq. (1). The larger  $\eta$  beam spin asymmetry measurements, however, suggest that the interference terms between chiral-even and chiral-odd GPDs are not well understood. Additionally, the correlation between  $Q^2$  and  $x_B$  coverage originated from the geometrical acceptance of CLAS detector prohibits one to make a definite conclusion about  $Q^2 - x_B$  dependencies.

The flat behavior of the  $-t$  dependence is related to the joint contribution of chiral-odd and chiral-even terms and is strongly determined by the interplay between the GPDs  $\tilde{H}$  and  $E_T$ . The model calculations demonstrate that chiral-odd and chiral-even GPDs do not have a flat behavior in  $-t$ , but their product produces a flat slope. The aforementioned is valid for both the  $\pi^0$  and  $\eta$  channels. Since the underlying GPDs have different quark flavor combinations, the difference in magnitudes between the  $\pi^0$  and  $\eta$  beam spin asymmetries may provide insight into the  $u$  and  $d$  quark GPDs differences and particularly their signs. However, the detailed interpretation is complicated because the polarized structure functions contain a mixture of GPDs. The future combined analysis of our results, unpolarized structure functions, target and double spin asymmetries from DVCS and DVMP, will elucidate less known terms in the GPDs.

In conclusion, the beam spin asymmetry for deeply virtual  $\eta$  meson production was measured over a wide range of  $Q^2$ ,  $x_B$  and  $-t$  for the first time. The BSA measurements shown in Fig. 5 are significantly different from zero in all kinematic bins. These results are in contrast with the “traditional” description of the process in terms of GPDs at leading twist, which predicts a negligible contribution from transversely polarized photons and, therefore, a zero BSA. The first interpretation of the beam spin asymmetries for  $\eta$  meson production within the GPD formalism comes from the updated theoretical perspective that includes significant contributions from both longitudinal ( $\gamma_L^*$ ) and transverse ( $\gamma_T^*$ ) virtual photons. Comparison with the GK and GGL model calculations indeed shows the importance of our results to constrain the  $-t$  dependence of the GPD parameterization, and the strong sensitivity of the data to both chiral-odd and chiral-even GPDs with emphasis on  $\tilde{H}$  and  $E_T$ . These data, combined with the unpolarized structure function measurements and beam spin asymmetry

results for  $\pi^0$  from CLAS [18,19,32], provide new constraints to existing GPD models and play an important role in the future GPD quark flavor decomposition analysis.

### Acknowledgements

We thank the staff of the Accelerator and Physics Divisions at Jefferson Lab for making the experiment possible. This work was supported in part by the U.S. Department of Energy (No. DE-FG-04ER41309), the National Science Foundation, the French Centre National de la Recherche Scientifique and Commissariat à l'Énergie Atomique, the French-American Cultural Exchange (FACE), the Italian Istituto Nazionale di Fisica Nucleare (INFN), the Chilean Comisión Nacional de Investigación Científica y Tecnológica (CONICYT), the National Research Foundation of Korea, and the UK Science and Technology Facilities Council (STFC). Jefferson Science Associates (JSA) operates the Thomas Jefferson National Accelerator Facility for the United States Department of Energy under contract DE-AC05-06OR23177.

### References

- [1] X.-D. Ji, Gauge-invariant decomposition of nucleon spin, *Phys. Rev. Lett.* 78 (1997) 610–613.
- [2] A.V. Radyushkin, Nonforward parton distributions, *Phys. Rev. D* 56 (1997) 5524–5557.
- [3] D. Müller, D. Robaschik, B. Geyer, F.M. Dittes, J. Hořejší, Wave functions, evolution equations and evolution kernels from light ray operators of QCD, *Fortschr. Phys.* 42 (1994) 101–141.
- [4] M. Guidal, Extraction of Compton Form Factors from DVCS data, *PoS ICHEP2010* (2010) 148, <https://doi.org/10.22323/1.120.0148>.
- [5] S. Stepanyan, et al., CLAS Collaboration, Observation of exclusive deeply virtual Compton scattering in polarized electron beam asymmetry measurements, *Phys. Rev. Lett.* 87 (2001) 182002.
- [6] A. Airapetian, et al., HERMES Collaboration, Measurement of the beam-spin azimuthal asymmetry associated with deeply-virtual Compton scattering, *Phys. Rev. Lett.* 87 (2001) 182001, <https://doi.org/10.1103/PhysRevLett.87.182001>.
- [7] S. Chen, et al., CLAS Collaboration, Measurement of deeply virtual Compton scattering with a polarized proton target, *Phys. Rev. Lett.* 97 (2006) 072002.
- [8] H.S. Jo, et al., CLAS Collaboration, Cross sections for the exclusive photon electroproduction on the proton and generalized parton distributions, *Phys. Rev. Lett.* 115 (2015) 212003.
- [9] M. Defurne, et al., Hall A Collaboration, E00-110 experiment at Jefferson Lab Hall A: deeply virtual Compton scattering off the proton at 6 GeV, *Phys. Rev. C* 92 (2015) 055202.
- [10] F.X. Girod, et al., CLAS Collaboration, Measurement of deeply virtual Compton scattering beam-spin asymmetries, *Phys. Rev. Lett.* 100 (2008) 162002.
- [11] G. Gavalian, et al., CLAS Collaboration, Beam spin asymmetries in deeply virtual Compton scattering (DVCS) with CLAS at 4.8 GeV, *Phys. Rev. C* 80 (2009) 035206.
- [12] A. Airapetian, et al., HERMES Collaboration, Measurement of azimuthal asymmetries with respect to both beam charge and transverse target polarization in exclusive electroproduction of real photons, *J. High Energy Phys.* 06 (2008) 066.
- [13] A. Airapetian, et al., HERMES Collaboration, Measurement of double-spin asymmetries associated with deeply virtual Compton scattering on a transversely polarized hydrogen target, *Phys. Lett. B* 704 (2011) 15–23.
- [14] M.I. Eides, L.L. Frankfurt, M.I. Strikman, Hard exclusive electroproduction of pseudoscalar mesons and QCD axial anomaly, *Phys. Rev. D* 59 (1999) 114025.
- [15] L. Mankiewicz, G. Piller, A. Radyushkin, Hard exclusive electroproduction of pions, *Eur. Phys. J. C* 10 (1999) 307–312.
- [16] K. Goeke, M.V. Polyakov, M. Vanderhaeghen, Hard exclusive reactions and the structure of hadrons, *Prog. Part. Nucl. Phys.* 47 (2001) 401–515.
- [17] E. Fuchey, et al., Exclusive neutral pion electroproduction in the deeply virtual regime, *Phys. Rev. C* 83 (2011) 025201.
- [18] R. De Masi, et al., CLAS Collaboration, Measurement of  $ep \rightarrow ep\pi^0$  beam spin asymmetries above the resonance region, *Phys. Rev. C* 77 (2008) 042201.
- [19] I. Bedlinskiy, et al., CLAS Collaboration, Measurement of exclusive  $\pi^0$  electroproduction structure functions and their relationship to transversity GPDs, *Phys. Rev. Lett.* 109 (2012) 112001.
- [20] M. Defurne, et al., Hall A Collaboration, Rosenbluth separation of the  $\pi^0$  electroproduction cross section, *Phys. Rev. Lett.* 117 (2016) 262001.
- [21] A. Airapetian, et al., HERMES Collaboration, Single spin azimuthal asymmetry in exclusive electroproduction of  $\pi^+$  mesons, *Phys. Lett. B* 535 (2002) 85–92.
- [22] A. Airapetian, et al., HERMES Collaboration, Cross-sections for hard exclusive electroproduction of  $\pi^+$  mesons on a hydrogen target, *Phys. Lett. B* 659 (2008) 486–492.
- [23] S. Ahmad, G.R. Goldstein, S. Liuti, Nucleon tensor charge from exclusive  $\pi^{*0}$  electroproduction, *Phys. Rev. D* 79 (2009) 054014.
- [24] S.V. Goloskokov, P. Kroll, Transversity in hard exclusive electroproduction of pseudoscalar mesons, *Eur. Phys. J. A* 47 (2011) 112.
- [25] G.R. Goldstein, J.O. Gonzalez Hernandez, S. Liuti, Flexible parametrization of generalized parton distributions from deeply virtual Compton scattering observables, *Phys. Rev. D* 84 (2011) 034007.
- [26] G.R. Goldstein, J.O. Gonzalez Hernandez, S. Liuti, Flexible parametrization of generalized parton distributions: the chiral-odd sector, *Phys. Rev. D* 91 (2015) 114013.
- [27] D. Drechsel, L. Tiator, Threshold pion photoproduction on nucleons, *J. Phys. G* 18 (1992) 449–497.
- [28] M. Diehl, S. Sapeta, On the analysis of lepton scattering on longitudinally or transversely polarized protons, *Eur. Phys. J. C* 41 (2005) 515–533.
- [29] A. Bacchetta, M. Diehl, K. Goeke, A. Metz, P.J. Mulders, M. Schlegel, Semi-inclusive deep inelastic scattering at small transverse momentum, *J. High Energy Phys.* 02 (2007) 093.
- [30] A. Kim, et al., CLAS Collaboration, Target and double spin asymmetries of deeply virtual  $\pi^0$  production with a longitudinally polarized proton target and CLAS, *Phys. Lett. B* 768 (2017) 168–173.
- [31] P.E. Bosted, et al., CLAS Collaboration, Target and beam-target spin asymmetries in exclusive pion electroproduction for  $Q^2 > 1 \text{ GeV}^2$ . II.  $ep \rightarrow e\pi^0 p$ , *Phys. Rev. C* 95 (2017) 035207.
- [32] I. Bedlinskiy, et al., CLAS Collaboration, Exclusive  $\pi^0$  electroproduction at  $W > 2 \text{ GeV}$  with CLAS, *Phys. Rev. C* 90 (2014) 025205.
- [33] I. Bedlinskiy, et al., CLAS Collaboration, Exclusive  $\eta$  electroproduction at  $W > 2 \text{ GeV}$  with CLAS and transversity generalized parton distributions, *Phys. Rev. C* 95 (2017) 035202.
- [34] B.A. Mecking, et al., The CEBAF large acceptance spectrometer (CLAS), *Nucl. Instrum. Methods Phys. Res., Sect. A, Accel. Spectrom. Detect. Assoc. Equip.* 503 (2003) 513–553.
- [35] M. Mestayer, et al., The CLAS drift chamber system, *Nucl. Instrum. Methods Phys. Res., Sect. A, Accel. Spectrom. Detect. Assoc. Equip.* 449 (2000) 81–111.
- [36] M. Amarian, et al., The CLAS forward electromagnetic calorimeter, *Nucl. Instrum. Methods Phys. Res., Sect. A, Accel. Spectrom. Detect. Assoc. Equip.* 460 (2001) 239–265.
- [37] G. Adams, et al., The CLAS Cherenkov detector, *Nucl. Instrum. Methods Phys. Res., Sect. A, Accel. Spectrom. Detect. Assoc. Equip.* 465 (2001) 414–427.
- [38] E. Smith, et al., The time-of-flight system for CLAS, *Nucl. Instrum. Methods Phys. Res., Sect. A, Accel. Spectrom. Detect. Assoc. Equip.* 432 (1999) 265–298.